Nanoscale

Accepted Manuscript

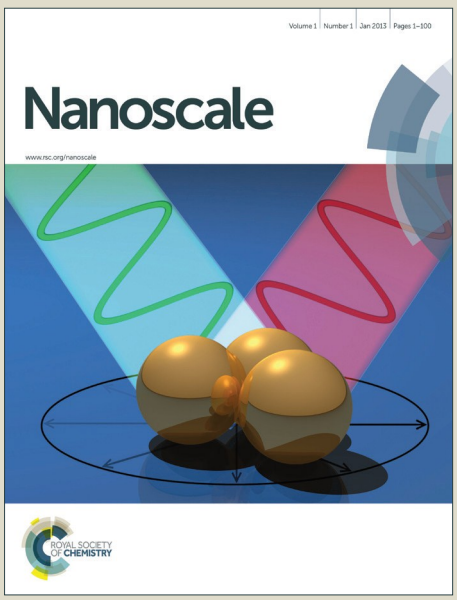

ROYAL SOCIETY OF CHEMISTRY

www.rsc.org/nanoscale

Nanoscale

ARTICLE

Cellular Recognition and Macropinocytosis-like Internalization of Nanoparticles Targeted to Integrin **α2β1**

Received 00th January 20xx,
Accepted 00th January 20xx

DOI: 10.1039/x0xx00000x

www.rsc.org/

P. Kankaanpää*,[a,b] S. Tiitta,[a,b] L. Bergman,[c] A-B. Puranen,[a,b] E. von Haartman,[c,e] M. Lindén[c,d] and J. Heino*[a,b]

Targeting nanoparticles to desired intracellular compartments is a major challenge. Integrin-type adhesion receptors ar- connected to different endocytosis routes in a receptor-specific manner. According to our previous observations, the internalization of an α2β1-integrin-echovirus-1 complex takes place via a macropinocytosis-like mechanism, suggestin that the receptor could be used to target nanoparticles to this specific entry route. Here, silica-based nanoparticles carrying monoclonal antibodies against the α2β1 integrin as address labels, were synthesized. Studies with flow cytometry, atomic force microscopy and confocal microscopy showed the particles to attach to the cell surface via the α2β1 inte Furthermore, quantitative analysis of nanoparticle trafficking inside the cell performed with the BioImageXD software indicated that the particles enter cells via a macropinocytosis-like process and end up in caveolin-1 positive structure Thus, we suggest that different integrins can guide particles to distinct endocytosis routes and, subsequently, also t specific intracellular compartments. In addition, we show that with the BioImageXD software it is possible to conduct sensitive and complex analyses of the behavior of small fluorescent particles inside cells, using basic confocal microscop images.

1 Introduction

The targets of many drugs are located in specific intracellular compartments. Therefore, medically used nanoparticles should not only bind to the cell surface and get internalized, but they should also find their way to the right location inside the cell.[1] The potential value of the human integrin family of cell adhesion receptors in intracellular nanoparticle targeting can be based on studies focused on the life cycles of viruses, since nanoparticles resemble viruses in many ways. For instance, integrins containing the αV subunit, a receptor for e.g. fibronectin and vitronectin, are used in the entry into cells by many adenoviruses,[2] coxsackievirus A9,[3-5] human parechovirus 1,[6] foot-and-mouth disease virus,[7] and Kaposi's sarcoma-associated herpesvirus (KSHV/HHV-8).[8, 9] αV integrins guide parechovirus 1 to clathrin-dependent endocytosis.[6] In contrast, echovirus 1 entry is critically dependent on the α2β1 integrin,[10, 11] a collagen receptor. Echovirus 1 takes advantage of macropinocytosis and accumulates into caveolin-1-positiv vesicles.[12-14] It can therefore be hypothesized that integrin binding address labels can be used not only for the selection o the right cell type, but also to target the particles to designated intracellular compartment. Integrin α2β1 has als been linked to the phagocytosis of collagen-coated beads b fibroblasts. However, also other collagen receptors (e.g discoidin domain receptors and endo180) may modify thi process.[15]

Previously, different members of the integrin family ha been used as nanoparticle binding receptors. Integrin αVβ3 can recognize a specific three-amino-acid residue motif, RGD, in its ligands. Nanoparticles have been guided to developin blood vessels in tumors *in vivo*, using small organic αVβ3 ligands[16] or cyclic RGD peptides.[17] RGD peptides can also guide nanoparticles to αVβ3 positive melanoma xenografts[18, 19] o glioblastoma cells.[20] Nanoparticles targeted to α5β1 integrin, a fibronectin receptor,[21-23] and α3β1 integrin, a lamini receptor,[24] have been published as well. In contrast, to our knowledge there are no available publications describin specific nanoparticle targeting to the α2β1 integrin, a receptor for collagen.

To study the intracellular trafficking of α2β1 integrin-guided particles, we prepared Stöber-like silica nanoparticles (diameter 70 nm) surface-conjugated with polyethylene glyco to achieve stealth features in cellular environments. Th particle surface was further modified with streptavidin and a α2β1 integrin-specific antibody for targeting the particles t α2β1 integrin-dependent endocytosis.

[a] *Department of Biochemistry, FI-20014 University of Turku, Turku, Finland.*
[b] *MediCity, University of Turku, Tykistökatu 6 A, FI-20520 Turku, Finland.*
[c] *Laboratory of Physical Chemistry, Åbo Akademi University, FI-20500 Turku, Finland.*
[d] *Present address: Inorganic Chemistry II, University of Ulm, Albert-Einstein-Allee 11, D-89081 Ulm, Germany.*
[e] *Pharmaceutical Sciences Laboratory, Åbo Akademi University, FI-20520* Turku, Finland.
Electronic Supplementary Information (ESI) available: nanoparticle characterization (Fig. S1), flow cytometry specificity tests of particles on CHO-cells (Fig. S2) and a supplementary video (Video S3) of nanoparticle internalization. See DOI: 10.1039/x0xx00000x

When studying the cellular interaction processes of small particles, it is important to use robust quantitative bioimaging, capable of producing reliable results from the relatively low resolution and low intensity image data often associated with such experiments. In this work we wanted to develop methods to quantify the cell surface attachment and subsequent internalization and localization of nanoparticles, using basic fluorescence confocal microscopy and freely available, established software tools. BioImageXD has been specifically developed for scientific bioimage processing and is capable of a wide range of image analysis functions run in large batches.[26] We have previously used BioImageXD to study integrin clustering and internalization with robust protocols validated with simulated data.[26] Now, we applied similar protocols to analyze nanoparticle entry, and devised a sensitive colocalization analysis to follow their intracellular fate.

We successfully analyzed the intracellular trafficking of α2β1 integrin-targeted nanoparticles with confocal microscopy and BioImageXD. Our results from confocal microscopy, flow cytometry and atomic force microscopy (AFM) experiments indicate that α2β1-targeted nanoparticles undergo a similar entry process as echovirus 1, from the first attachment to the cell membrane to the fate in the intracellular compartments. We also showed that BioImageXD is an optimal toolkit to quantitatively study the internalization of fluorescent particles.

2 Results and discussion

2.1. Nanoparticle characterization

Partially amino-functionalized silica nanoparticles with a mean diameter of approximately 70 nm (as determined by SEM) were first synthesized using a mixture of aminotrimethoxysilane (APS) and tetraethoxysilane (TEOS). Fluorescein isothiocyanate (FITC) was covalently incorporated into the particle structure during particle synthesis by conjugating it to APS primary amino groups. Surface modification was done by using homobifunctional α,ω-Bis-NHS-PEG, Mw 3000 as a crosslinker between the particle surface amino groups and the fluorescent streptavidin amino groups. PEG was used in order to provide steric stability and to minimize unspecific protein adsorption to the particles. In a typical conjugation procedure, particles were dispersed in MES buffer, pH 5.2, α,ω-Bis-NHS-PEG was added and let react for 15 minutes, thereafter fluorescent streptavidin was added and the conjugation was allowed to proceed for 1.5 hours. The intensity-weighted hydrodynamic size of the particles after the attachment of PEG, as determined by dynamic light-scattering, was about 130 nm, with a polydispersivity index (PDI) of 0.08 (Fig. S1a). After attachment of PEG-streptavidin to the surface, the hydrodynamic size increased to about 170 nm, with a PDI of 0.124 (Fig. S1b). The synthesized nanoparticle system is schematically represented in Figure 1a, and a scanning electron microscopy (SEM) image of the particles is shown in Figure 1b.

The surface modifications can easily be followed with zeta potential measurements. Amino-FITC functionalized particles

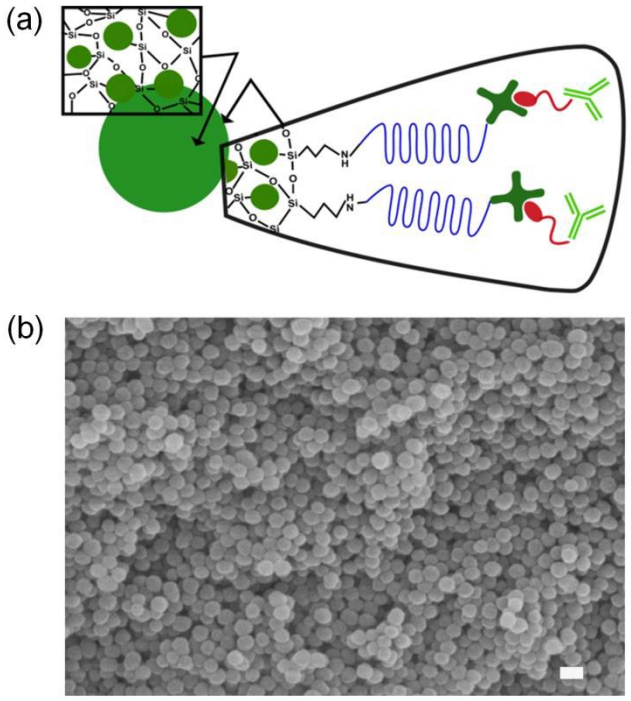

Fig. 1. Silica-based nanoparticles with antibodies as biological address labels. a. Schematic representation. Fluorescent isothiocyanate (FITC) is shown incorporated in the silica network, polyethylene glycol is conjugated to the surface amino groups, and the surface is further conjugated with streptavidin and biotinylated antibody against α integrin. b. Scanning electron microscopy image taken prior to surface-modification steps of the prepared Stöber-like nanoparticles. Scale bar 100 nm.

were measured to have a zeta potential of 30 mV, which increased to 42 mV after the PEG-streptavidin surface modification (100 mM MES, pH 5.2). The pI of streptavidin is depending on the reference, in the range 5-7. After conjugation of streptavidin the zeta potential of the particles increases, which indicates successful surface functionalization.

2.2 Particle targeting to sarcoma cell surface

A human osteosarcoma cell line (Saos-2) stably expressing α2β1 integrin (α2 Saos-2) was used as a model system to study particle interactions with cells.[27] The particles used in these experiments were conjugated to biotinylated antibodies either a monoclonal antibody against the integrin α2-subunit ("α2-particles") or a negative control antibody 3G6 ("control particles") against chicken T cells (the epitope is not present in the cell type used). First we incubated α2-particles or control particles with the cells for approximately 30 min, and after washing we investigated the amount of cell-bound particles with flow cytometry. As shown in Figure 2a, the α2-particles were specifically bound to the cells, whereas control particles showed only weak binding, similar to cell type-dependent background levels. Next, we wanted to confirm that the attachment of α2-particles was specific for α2 integrin, and compared the attachment of α2-particles to α2 Saos-2 cells with wild type Saos-2 (WT Saos-2) cells lacking α2 integrin by flow cytometry (Fig. 2b). Indeed, α2-particles bound more specifically to α2 Saos-2 cells than to WT Saos-2 cells (these results were also confirmed by the results obtained by quantitative microscopy in Figure 5a). We then fixed cells with

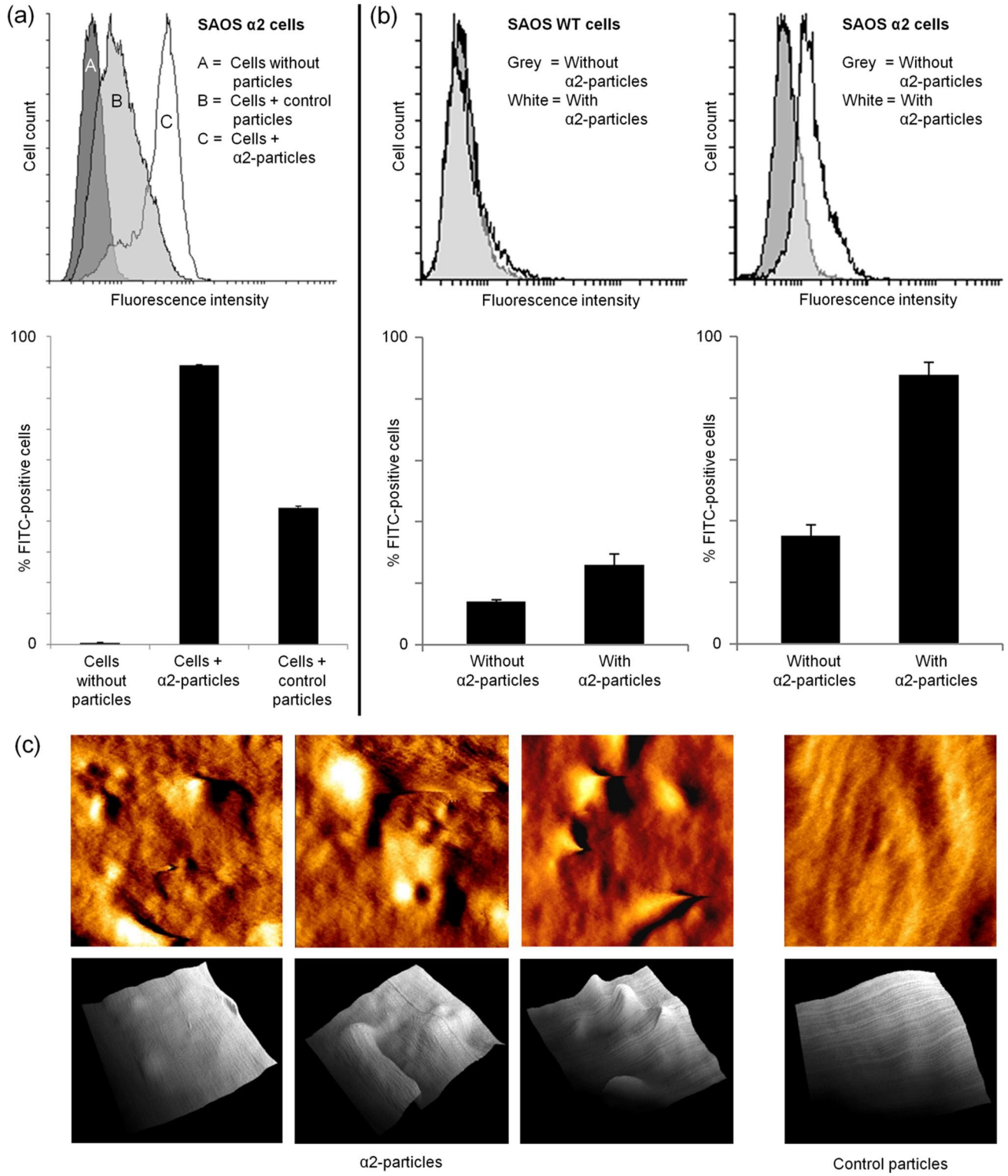

Fig. 2. Particles were specifically bound to α2β1 integrin-positive cell surfaces. a-b. Upper charts: Flow cytometry volume plots of individual experiments, lower charts: flow cytometry bar charts counted as the mean of two parallel samples. a. Comparison of α2- and control particle attachment. Flow cytometry volume plot (upper chart) and bar chart (lower chart) showing attachment of α2-particles to the surface of α2 Saos-2, cells with control particles showing very little attachment in the volume plot. The bar chart displays results of two repeated experiments, showing that α2-particles attached to the cell surface considerably more than control particles. b. Comparison of α2-particle binding to WT (left) and α2 (right) Saos-2 cells. Flow cytometry volume plots (upper charts) and bar charts (lower charts) showing attached particles to cells lacking α2 integrin (WT) and to cells stably transfected with α2 integrin, with very few particles attaching to WT Saos-2 cells as compared to α2 Saos-2 cells (upper charts: volume plots). Samples without particles have no added fluorophores and describe the fluorescence background in each cell line. c. Typical atomic force microscopy images showing a speckled cell surface with α2-particles and a smooth surface with control particles. Upper row shows vertical deflection images, which highlight the edges of structures, and lower row shows topography images (3D warp scalar renderings created with BioImageXD). Each image is a 2 x 2 μm area of the cell surface.

PFA, and imaged their surfaces in PBS with atomic force microscopy, using low force contact mode with soft cantilevers to detect surface topography without disturbing it. Figure 2c shows that cells incubated with α2-particles had speckled surfaces indicative of particle binding, whereas cells incubated with control particles showed smoother surfaces similar to a cell surface under normal conditions.

Next we looked at the cell surface with 3D confocal microscopy, to confirm that the attachment of α2-particles to the surface took place via the α2β1 integrin. As the particles contained FITC, they were fluorescent, and α2β1 integrin was made fluorescent by immunolabeling with Alexa 555-coupled secondary antibodies after labeling with a primary antibody of different species than the antibody used in the nanoparticles. Particle concentration was kept high enough for also some unspecific binding of the control particles to the cell surface to take place. In this way both particle types could be analyzed for colocalization with the integrin. Importantly, the amount of control particles on the cell surface still remained substantially smaller than that of α2-particles despite the fact that the cells were treated with an equal concentration of both control and α2-particles. As shown in Figure 3a, α2-particles showed clear colocalization with α2β1 integrin, whereas control particles did not. We devised a method for quantitative colocalization analysis, wherein colocalization was quantified by segmenting the particle channel, and then calculating the ratio of the integrin channel intensity within the segmented particles to elsewhere in the cell. This way the colocalization could be measured with high sensitivity even in cases where there were only a few voxels with strong signal in one of the channels (such as the typical case of having only a small amount of particle signal with control particles compared to the large amount of α2β1 integrin signal). A result of 1 would indicate the same amount of integrins at the particle sites as elsewhere in the cell, and therefore no colocalization, whereas a number larger than 1 would indicate higher amount of integrins at the particle sites than elsewhere. Cells were fixed and analyzed after 15 min and 60 min incubation with the particles, and as seen in Figure 3b, both time points showed values close to 1 with the control particles, whereas α2-particles showed significant colocalization with the α2β1 integrin.

Our results confirmed that the α2 antibody-containing nanoparticles could be specifically targeted to α2β1 integrin positive cells. Previous studies have shown similar targeting distinctly to αV integrins, α5β1 integrin and α3β1 integrin.[16, 21, 24] Integrin α2β1 is normally expressed for instance on epithelial cells and activated T lymphocytes.[28, 29] Interestingly, many malignant cells, including prostate cancer stem cells, are also α2β1 positive.[30] Furthermore, α2β1 is expressed on endothelial cells during active angiogenesis[31] and on many inflammatory cells.[32] Thus, α2β1-binding nanoparticles have potential use in treating many human diseases.

2.3. Particle clustering on the cell surface

We have previously shown α2β1 integrin to form clusters on the cell surface upon binding to for instance a combination of primary and secondary antibodies or human echovirus 1,

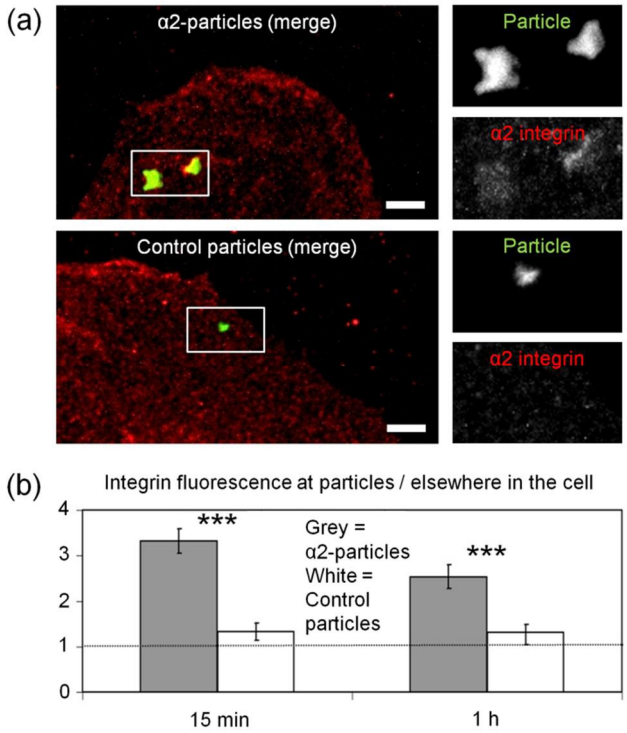

Fig. 3. Particles colocalized with α2β1 integrin on the cell surface. a. Typical confocal microscopy images showing the colocalization between α2-particles (green) and α2β1 integrin (red), and control particles having no such colocalization. Scale bar 5 μm. b. The colocalization was quantified by segmenting the particle channel, and then calculating the ratio of the integrin channel intensity within the segmented particles to elsewhere in the cell. There was significantly more integrin signal at the α2-particles than elsewhere in the cell, but no such difference with the control particles. Statistical significance symbols indicate differences between control particles and α2-particles, as measured with t-tests.

which uses the integrin as its receptor in cell entry.[13] This clustering is most likely part of the normal behavior of the integrin, similar to the clustering behavior of many other cell surface receptors, and an elemental part of the integrin internalization process. We therefore wanted to study whether the nanoparticles with α2 antibody could also induce such clustering. Particle concentration was doubled for these experiments, to allow for more unspecific control particle binding, so that the clustering effect between samples could be properly compared. We stained the cell volume with CellTracker Orange and analyzed nanoparticle clusters (FITC stain) by segmenting both them and the cell membrane,[26] for the 15 min time point at which the clusters are typically very prominent. We quantified three central parameters for the clusters: intensity, volume and number per cell surface area. During clustering the first two should increase, whereas the last one should decrease.[26] Indeed, as shown in Figure 4, clusters of α2-particles were much brighter and larger but fewer in number than those of control particles. α2-particles thus clustered significantly more on the cell membrane than control particles, probably indicative of the underlying integrin clustering. As shown before, integrin clustering cannot be initiated with fluorophore-coupled primary antibodies against the α2 integrin. Only the use of an additional set of (secondary) antibodies induces cluster formation.[13] The fact that our nanoparticles, attached to primary antibodies, were

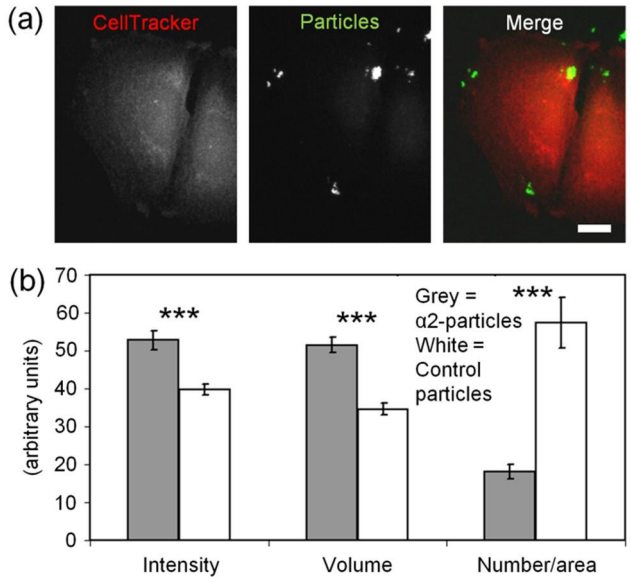

Fig. 4. Particles formed clusters on the cell surface via α2β1 integrin. a. Typical confocal microscopy images of the clusters formed by α2-particles (green) on the cell surface (red). Scale bar 5 μm. b. Quantification of the particle clusters, which were significantly larger, brighter and fewer in number with α2-particles than with control particles, all indicating stronger clustering with α2-particles than with control particles. Statistical significance symbols indicate differences between control particles and α2-particles, as measured with t-tests.

able to cluster the α2 integrin also reflects the multivalent nature of our particles. Consequently, this clustering ability of the particles also confirmed that the particles were attaching to the integrins in a manner that could potentially trigger also their internalization.

The result also showed that the protocol for BioImageXD, previously optimized for the analysis of integrin clusters, could be applied also to the analysis of nanoparticles. The protocol was originally designed to be able to deal with clustering integrins, whose many parameters, such as size and intensity, vary substantially over time.[26] This enabled it to be used also with the nanoparticles, and its robustness and previous validation bring added reliability to the nanoparticle analysis.

2.4. Internalization of the nanoparticles

We have previously shown that while forming clusters, α2β1 integrin is also internalized into the cell.[13, 26] Echovirus 1 is capable of forming these integrin clusters in a similar manner, and uses this mechanism for its cellular entry.[10, 12] We used 3D confocal microscopy to study whether the nanoparticles would be similarly internalized. Both the particles and the cell membrane were segmented from the images. The increase in total number of voxels internalized and the increase in percentage of voxels internalized were calculated.[26] As shown in Figure 5b, more α2-particles (dark grey bar) than control particles (white bar) were internalized after 1 h of particle incubation. With time the percentage of internalized particles increased, and the increase was larger with α2-particles than control particles. The experiment was repeated with doubled particle concentration (as in the clustering studies shown in Figure 4; Figure 5b black and light grey bars), to enable more control particles to be analyzed, and to see whether specific internalization could still be observed also at higher particle concentrations. As was to be expected, there was increased unspecific entry of the control particles, but significantly more internalization was still observed with α2-particles, and the increase in internalization over time was also still higher with the α2-particles.

As with clustering, previously established BioImageXD protocols for integrin analyses[26] were successfully applied to quantify nanoparticle internalization. This approach has several advantages, such as that the same basic image data as used for simpler calculations like cluster number, can be used to quantify internalization. No additional staining or experiments are required. This makes a seemingly complex analysis fast and efficient to calculate. The analysis has also been extensively validated and proven functional.[26] However, as the resolution of the conventional light microscope is fairly low, the method may be inaccurate especially in cases where internalized particles would remain close to the membrane. Luckily this is often not the case, and good results can be obtained, as here. Despite the resolution aspect, the analysis is sensitive and can also detect differences not easily seen from the images by eye.

The specific internalization of the α2-particles was further confirmed with flow cytometry, wherein outside fluorescence was quenched with Trypan blue and thus only the fluorescence from internalized particles recorded. Figure 5c shows that significantly more α2-particles than control particles were internalized. Interestingly, in comparison to the flow cytometry results in Figure 2a, only a small portion of the cell surface bound control particles seemed to be internalized when compared to the same ratio for α2-particles. This suggests that even though there is some unspecific surface binding of the control particles, the endocytosis of the particles is more specific than the surface-binding event. In turn, this would support the usefulness of targeting nanovehicles to endocytic receptors for effective endocytosis.[33]

We wanted to confirm by visual observation in living cells, that the particles could actually be seen going into a cell. We recorded 4D confocal microscopy time series from living cells starting imaging before the particles were added to the incubation medium and continuing for more than 1 h after that. After imaging, we used surface rendering to visualize the cell surface based on the CellTracker stain, and surface rendered the particles similarly. We utilized the 3D rendering and animation capabilities of BioImageXD,[26] which include features such as simultaneous rendering of several modules and adjusting the virtual camera viewing angle to be very wide. These properties enable multi-channel views from inside small enclosures such as cells to be created. We could then observe what happened during the time series inside the cell and we could see the particles coming in through the cell membrane in increasing amounts (Fig. 5d and Video S3). This confirmed that the particles did indeed go inside living cells similarly to as seen with the fixed cell samples.

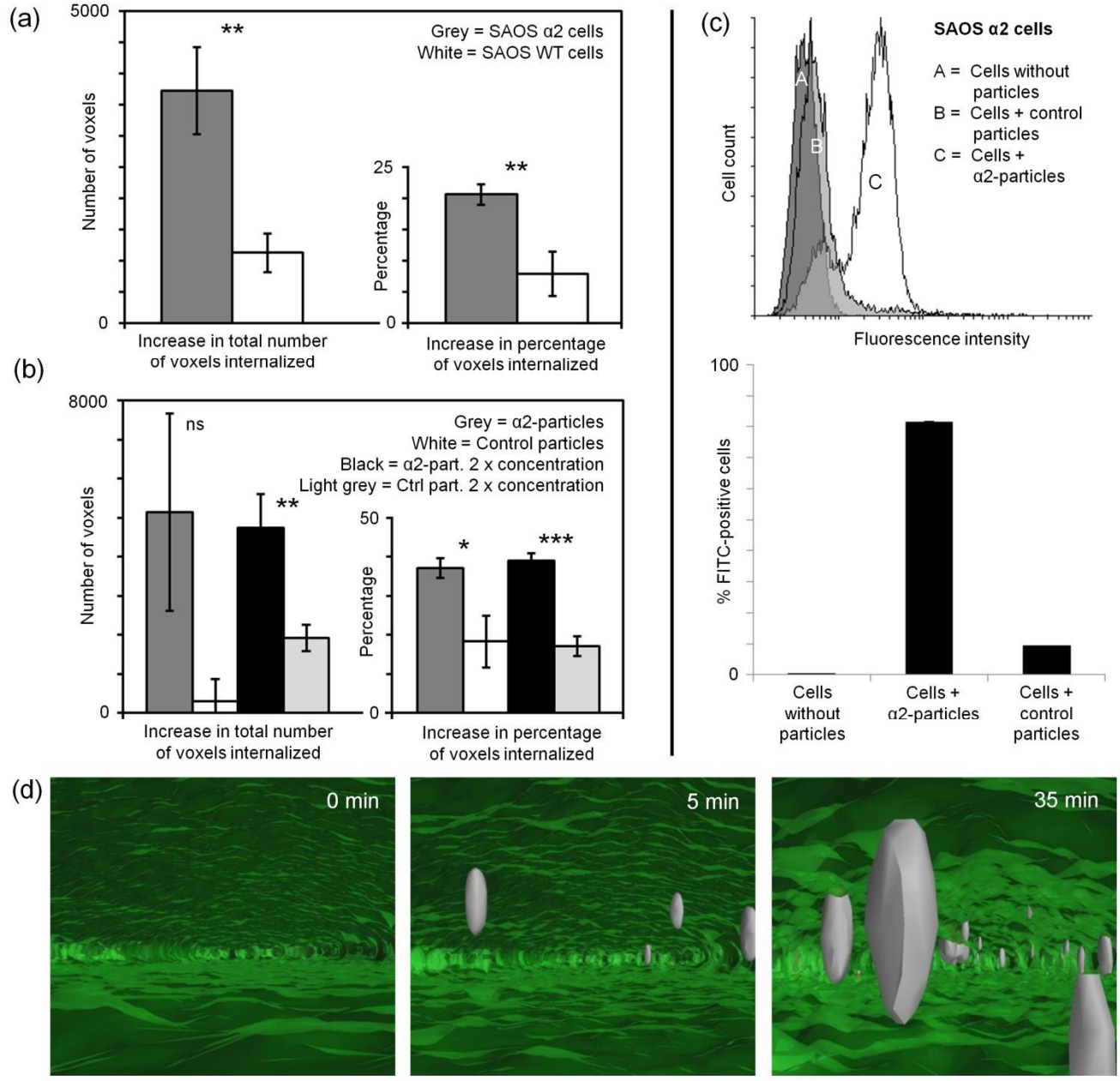

Fig. 5. Particles were specifically internalized into cells via α2β1 integrin. a. A significantly larger amount of α2-particles was found to internalize into α2 Saos-2 cells (grey) than into wild type cells (white) lacking α2 integrin. b. More α2-particles were also internalized over time into α2 Saos-2 cells, as compared to control particles, and the increase in the internalization percentage over time was also larger with α2-particles. In the high (2x) concentration samples, despite more unspecific binding, α2-particles were still internalized more. Experiments in a. and b. were performed with quantitative microscopy. Statistical significance symbols indicate differences between control particles and α2-particles, as measured with t-tests. c. Flow cytometry volume plot and corresponding bar chart showing considerably more internalization of α2-particles than control particles. (Non-internalized surface-bound particles were quenched with Trypan blue.) d. 3D surface rendering of a time series from inside a living cell, showing the entry of nanoparticles (grey) through the cell membrane (green). Rendered with BioImageXD.

Based on previous studies with human echovirus 1 and clustering integrin antibodies,[13, 26] we could predict that also nanoparticle-mediated integrin clustering could in principle trigger the entry machinery, but there was a possibility that the larger size of the silica-based nanoparticles could cause problems. However, as our results clearly indicate, after binding to α2β1 integrin, the nanoparticles were quite rapidly internalized. Echovirus 1 seems to favor non-activated integrins and avoid conformational changes in the receptor.[1] Still, the clustering of integrins alone can activate critical signaling pathways such as PKCα.[13] It can therefore be speculated that a nanoparticle can be similarly internalized, even if the address label does not mimic a natural ligand or otherwise activate a conformational change in the integrin.

2.5 Intracellular trafficking of **α2β**1 integrin targeted nanoparticles

Finally, we wanted to clarify the mechanism of the specific internalization of the α2-particles. Such studies are not always straightforward, as both natural nanoparticles such as viruses and especially artificial nanoparticles are most likely internalized through multiple routes, both specifically and

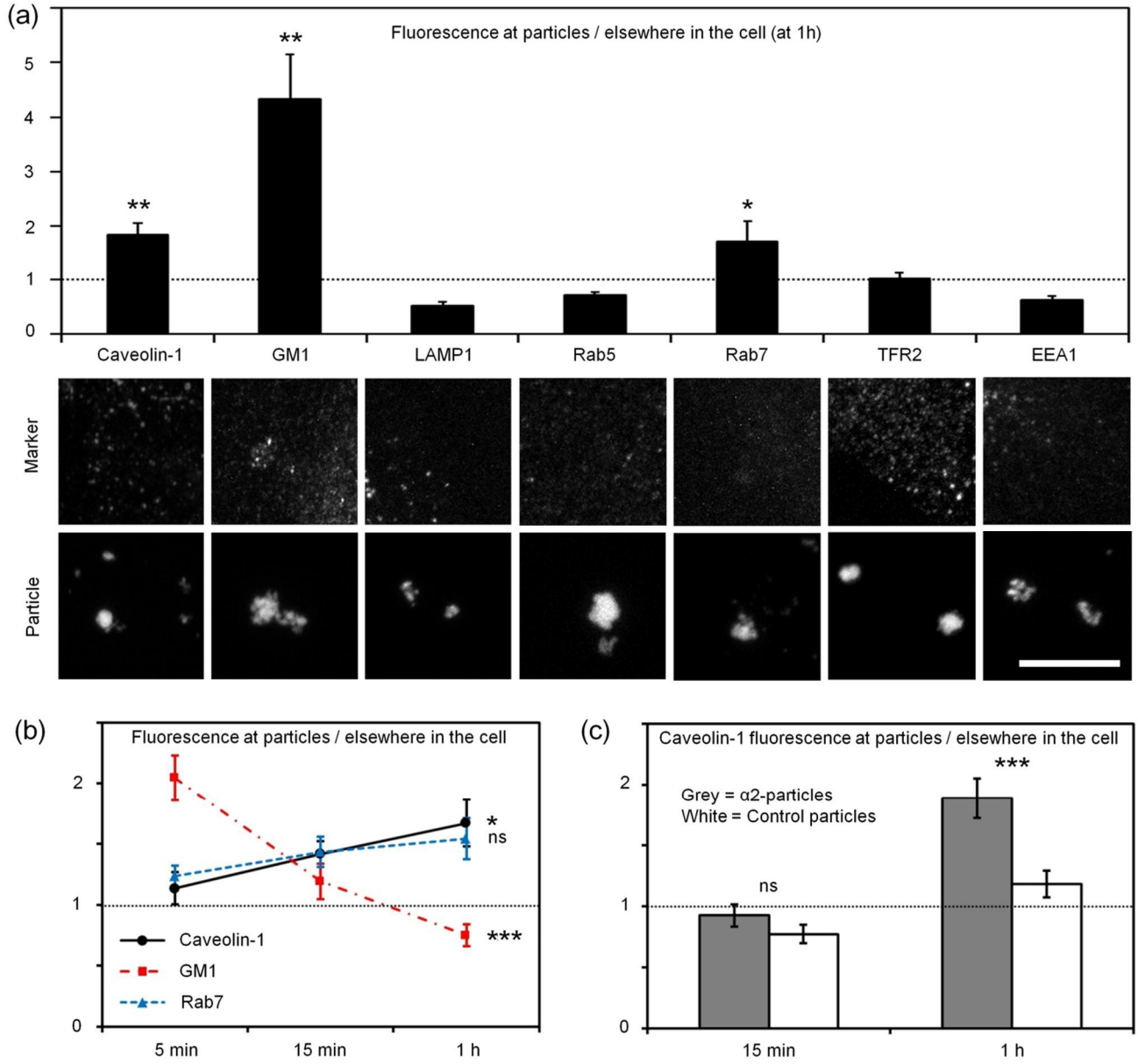

Fig. 6. a. Particles internalized via specific route(s) characteristic of α2β1 integrin-mediated internalization. At the top fluorescence ratios for each marker at the particles to elsewhere in the cells. A value greater than 1 corresponds to a significant co-localization. Statistical significance symbols indicate the difference between fluorescence intensity at the particles and elsewhere in the cells, as measured with t-tests, for those markers that showed any such difference. In the middle typical confocal microscopy images of the markers (1 h time points) and at the bottom the corresponding particle images. Scale bar 5 μm (same scale for all images). b. The co-localization of the α2-particles with caveolin-1 and Rab7 increased over time, whereas the highest co-localization between α2-particles and GM1 was seen at the earliest time-point (5 min). Here, unlike in other experiments, the nanoparticles allowed to attach to cells on ice, prior to incubation at 37 °C. Statistical significance symbols indicate differences between the first and last time points for each marker, as measured with t-tests. c. Control particles do not significantly co-localize with caveolin-1. The co-localization of α2-particles with caveolin-1 was compared to the co-localization of control particles with caveolin-1. Statistical significance symbols indicate differences between control particles and α2-particles, as measured with t-tests.

unspecifically.[34, 35] Sometimes clear positive colocalization results may not be obtained with any internalization marker,[36] possibly because colocalization signals are weak and too widely spread between different markers to be detected. We utilized the above-mentioned sensitive colocalization assay and assessed α2-particle colocalization with 7 known internalization markers: caveolin-1 for the caveolar pathway; monosialotetrahexosylganglioside (GM1) for the macropinocytosis pathway; Transferrin 2 (TFR2), Rab5 (early endosomes) and Early endosome antigen 1 (EEA1) for the clathrin-mediated pathway; Rab7 for late endosomes; and Lysosomal-associated membrane protein 1 (LAMP1) for late endosomes and lysosomes. Each marker was visualized with antibodies linked to the Alexa-555 fluorescent dye, and images one-by-one together with the fluorescent nanoparticles. All markers were imaged after 1 h of incubation with the nanoparticles. With EEA1 a 4 h time point was used in addition, to check for a possible slower clathrin-mediated mechanism (data not shown).[36]

Integrin α2β1 participates, together with other collagen receptors, in the phagocytosis of collagen-coated beads by fibroblasts.[15] Human echovirus 1 has no other cellular receptors than α2β1 and the virus/integrin complex is sho

to internalize via a macropinocytotic mechanism into caveolin-1 positive structures and further into late endosomal structures.[12-14] In accordance with this, α2-particles colocalized significantly with the macropinocytosis marker GM1, caveolin-1 and Rab7, a late endosome marker, as shown in Figure 6. Negative results were obtained with markers of the classical clathrin-dependent pathway (Transferrin 2 [TFR2], LAMP1, Rab5, EEA1). These types of markers typically produce negative results also with α2β1 integrin internalization.[13] In Figure 6b, we further investigated the time-scale of the positive co-localizations with a pulse-chase type of experiment. Notably, unlike in other experiments, the nanoparticles were allowed to attach to the cells on ice, prior to incubation at 37 °C. We found that the co-localization of α2-particles with GM1 is highest in the initial time-point (5 min). In contrast, co-localization with caveolin-1 and Rab7 is quite low after 5 min incubation, but increases during the rest of the 1h experiment. In addition, when we compared the co-localization of caveolin-1 with control and α2-particles, we found a significantly higher amount of the cellular caveolin-1 co-localizing with α2-particles than with control particles (Fig. 6c). Thus, our results suggest that the α2-particles were specifically internalized via the α2β1 integrin specific pathway(s). The result also indicates that our colocalization analysis method not only can detect signals from very few voxels, as explained above, but that it can possibly also detect differences between internalization routes in cases where multiple routes are operating at the same time, and traditional analyses may not be suitable.

To further assess the role of macropinocytosis in nanoparticle entry, we wanted to block macropinocytosis and subsequent nanoparticle entry. Since no exclusively selective inhibitor for macropinocytosis exist, we chose four different molecules, all generally used for macropinocytosis inhibition: 5-(N-Ethyl-N-isopropyl)amiloride (EIPA), LY294002, U-73122 and IPA 3. Our first choice was EIPA, an inhibitor of the Na^+/H^+ pump, which is claimed to have the fewest off-target effects.[37] This inhibitor also gave the clearest inhibition of particle internalization, and was the only inhibitor which showed a statistical difference in both the counted number of internalized voxels and the increase in internalization percentage. Of the rest, IPA 3 (group I p21-activated kinase (PAK) inhibitor) had the most profound effect on the increase in internalization percentage after EIPA, followed by U-73122 (phospholipase C inhibitor) and LY294002 (PI3K inhibitor). In fact, LY294002, which had the weakest effect, has previously been reported to incompletely block macropinocytosis in the used Saos-2 cell type.[14] To conclude, these results together with the results in Figure 6, support a role for macropinocytosis in the initial uptake of our particles.

As different integrins are known to internalize via different routes, for instance αV integrins use the clathrin-mediated pathway,[6] we propose that targeting different integrins might enable nanoparticles to be guided to different cellular entry routes. Indeed, we have also previously shown α2 and αV integrin clusters, similar to those observed in this study, to internalize via different routes into particular cellular compartments.[13]

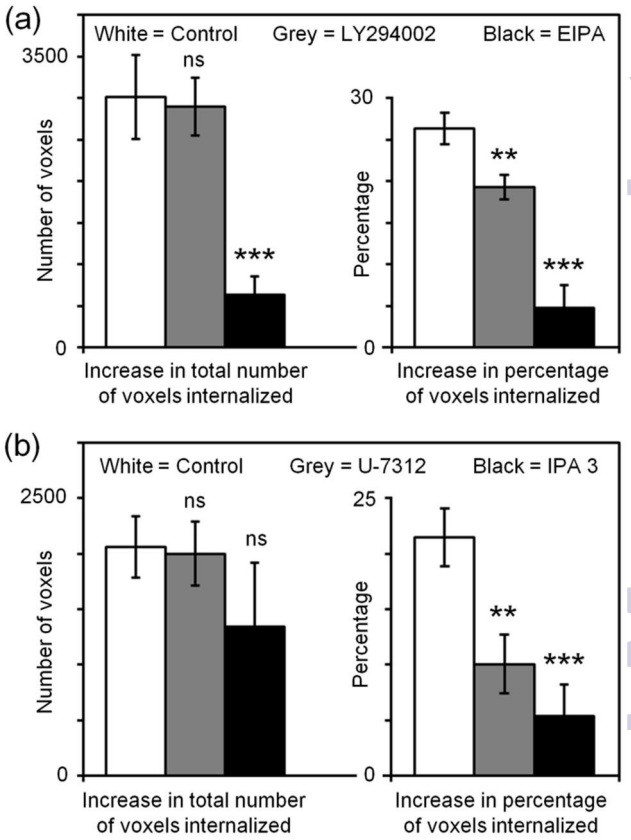

Fig. 7. Particle uptake into cells was reduced after inhibition of macropinocytosis. a-b Left panel: internalization counted by the increase in total number of voxels internalized, Right panel: internalization increase in percentage of voxels. a. The internalization of objects in EIPA (Amiloride derivative, inhibits sodium transport and blocks the Na+/H+ exchange pathway) and LY294002 (PI3K inhibitor) treated cells was compared against untreated cells. b. The internalization of objects in U-73122 (phospholipase C inhibitor) and IPA 3 (group I p21-activated kinase (PAK) inhibitor) treated cells was compared against untreated cells. Statistical significance symbols indicate differences between untreated control cells and cells treated with inhibitors, as measured with both ANOVA and t-tests.

Integrin α2β1 is expressed in various disease-associated cell types, including activated lymphocytes, neoangiogenesis-related endothelial cells and cancer cells.[38] Furthermore, antibodies against this integrin are in phase II clinical trials (Vatelizumab; www.glenmarkpharma.com). Thus, also nanoparticles targeted to this integrin could potentially be used in drug delivery in many human diseases, such as inflammation and cancer. The fact that the α2β1 integrin transports nanoparticles to a specific entry route can create new opportunities for the design of the particles, e.g. when the aim is to release the cargo inside a Rab7-positive compartment, presumably representing a late endosome.[3] Finally, our experiments indicate that, advanced quantitative bioimaging software, such as BioImageXD, can enable studies on nanoparticle trafficking.

3. Experimental

Synthesis of nanoparticles

The solid silica particle core was prepared based on the procedure decribed by Stöber et al.[25] In a typical synthesis, 250 μg (1mg ml^{-1}) of fluorescein isothiocyanate isomer I (FITC; minimum 90% HPLC, Sigma-Aldrich) was mixed with 3-aminopropyltriehtoxysilane (APTS; Sigma-Aldrich) under inert atmosphere and added to an alkaline (Ammonium hydroxide solution, max 33% NH_3, puriss., Sigma-Aldrich) solution together with tetraehoxyothosilicate (TEOS; purum ≥98% GC, Fluka). The resulting synthesis mixture had a molar ratio of 0.01 FITC : 17 APTS : 218 TEOS : 783 NH_4OH : 26674 EtOH. The sol was stirred over night at RT. On the next day the particles were separated by centrifugation and dried under vacuum at RT. The particles were further conjugated with polyethyleneglycol, PEG, (O,O′-Bis[2-(N-Succinimidyl-succinylamino)ethyl]polyethylene glycol Mw 3000, Sigma-Aldrich) and streptavidin Alexa fluor 488 conjugate (Molecular Probes; S11223), where the Alexa fluor provided improved photo stability for live cell confocal imaging. In a typical conjugation procedure, 5 mg of the prepared partially amino functionalized nanoparticles were dispersed in MES buffer (pH 5.2), 1 mg of α,ω-Bis-NHS-PEG, was added and stirred for 15 minutes, thereafter 17 μg of fluorescent Alexa fluor 488 was added to the reaction, and the conjugation was allowed to proceed for 1.5 hours. The particles were then separated by centrifugation, washed carefully 3 times, and finally dispersed (1 mg ml^{-1}) in water. Dynamic light-scattering (DLS) and zeta-potential measurements were performed using a Nano ZS (Malvern, UK) setup in a MES buffer. Measurements were performed at 298 K, using a monochromatic laser with a working wavelength of 632.8 nm, and using Non-Invasive Back-Scatter (NIBS) with the detector positioned at 173 relative to the laser beam. Scanning electron microscopy (Jeol JSM-6335F, Jeol Ltd., Japan) was performed by 50 k magnification, using an acceleration voltage of 10 kV, and a working distance 14.6 mm.

Particle coupling to biotinylated antibody

The streptavidin-conjugated particles (1 mg ml^{-1}) were coupled to biotinylated α2 integrin antibody (coupling solution 80 μg ml^{-1}; Serotec; MCA-2025) or to biotinylated negative control antibody 3G6 (monoclonal mouse antibody against chicken T cells)[40] (a kind gift from Professors Sirpa Jalkanen and Marko Salmi, University of Turku) under vigorous shaking for 1-2 h at RT. The particles were centrifuged (fast spinning down, 14.1 rcf, 4 minutes, RT), washed twice with HEPES (25 mM) and diluted in HEPES for a 1 mg ml^{-1} concentration.

Cell culture, inhibitor and particle incubations

Human Saos-2 osteosarcoma cells (ATCC) stably expressing α2 integrin (α2 Saos-2 cells)[27] were cultured under neomycin (Gibco; G418) selection. Both wild-type (WT) Saos-2 and α2 Saos-2 cells were maintained in DMEM supplemented with Fetal Calf Serum (10%; PromoCell), Ultraglutamine (Lonza), Streptomycin and Penicillin (Lonza) in a humidified chamber with 5% CO_2 at 37 °C. CHO WT and α2 integrin expressing cells[41] (α2 CHO) were cultured under same conditions in αMEM with the previously mentioned additives. F microscopy experiments, the cells were collected and split t 1/4th of original cell density two days prior to the experiment on no. 1.5 cover glasses (fixed samples) or glass bottom 8-wel plates (live cell samples). The cells were incubated with 125 μ ml^{-1} particles (or in experiments with higher concentration 250 μg ml^{-1}) in cell culture media at 37 °C for 15 min, 1 h or 4 together with 0.75 μM Celltracker Orange CMRA in the clustering, internalization and macropinocytosis inhibitio experiments (C34551; Molecular Probes; total incubation time 1 h for all samples). In the macropinocytosis inhibition experiments the inhibitors (EIPA, Sigma-Aldrich A3085, 50 μM; IPA 3, Tocris Bioscience 3622, 10 μM; LY294002, Calbiochem 440202, 50 μM; U-73122, Calbiochem 662035, 10 μM) wer added 1 h prior to the experiment together with th Celltracker dye. In the pulse-chase experiment, the cells wer kept on ice 15 min after the addition of nanoparticles, t washed and incubated at 37 °C for 5, 15 or 60 minutes. In al experiments, the cells were finally washed with PBS, and fi 20-30 min in 4% (w/V) PFA in PBS at RT.

Immunocytochemistry and confocal microscopy

After fixation, the cells were permeabilized with 0.2% Triton X 100 in PBS for 5 minutes, washed twice in PBS and incubate 1h at RT with primary antibodies against integrin α2 (R&D systems; MAB12332 1 μg ml^{-1}), Rab5 (Abcam; ab18211 1 μg ml^{-1}), TFR2 (Abcam; ab80194 5 μg ml^{-1}), GM1 (Calbiochem 345757 1 μg ml^{-1}), caveolin 1 (Abcam; ab24170 1 μg ml^{-1}), EEA1 (Abcam; SAB4500839 1 μg ml^{-1}) or Rab7 (Abcam ab77993 1 μg ml^{-1}). After washing (PBS; 3 x 5 min), samples were incubated 30 minutes at RT with Alexa Fluor 555 goa anti-rat (5 μg ml^{-1}; Molecular Probes; A21434) or goat anti-rabbit (5 μg ml^{-1}; Molecular Probes; A21429) and washed agai (4 x 5 min). All antibodies were diluted in (3% w/V) BSA/PBS. Samples were mounted with Mowiol-solution supplemente with DABCO (25 mg ml^{-1}). The samples were imaged with a Carl Zeiss Axio Observer.Z1 equipped with an LSM 510 confocal module with 3 PMT detectors (Carl Zeiss, Germany). A plan-apochromat oil immersion 63x 1.4 objective was used Voxel density was optimized according to the Nyquist theorem for every image. All acquisition parameters (such as detector sensitivity) were kept constant for all comparable samples, an at values that result in no saturation. Separate scanning of each wavelength (multi-tracking) and bleed-through tests of the filters and dichroics used were conducted in order to make sure the different fluorescence channels did not interfere with each other.

Live cell 4D confocal microscopy

The particles used for the live cell imaging experiment were synthesized without FITC and coupled to biotinylated antibody as described above, with the exception of conjugation to Alexa 555 streptavidin (Molecular Probes; S21381) instead of Alexa 488 streptavidin. Prior to the experiment, the cells were incubated 1.5 h with Celltracker Green CMFDA (0.5 μ

Molecular Probes; C2925) according to the manufacturer's instructions, and the media was changed to CO_2 independent media (Gibco). The confocal microscope was pre-heated at 37 ^{o}C 3 h before the experiment, the last 30 min with the cell plate in place. Sonicated particles were added to a final concentration of 40 μg ml^{-1} just before obtaining the second stack in a 90 min long time-series, with 3D image stacks acquired at 5 minute intervals. Voxel density and other acquisition parameters were adjusted as described above for fixed samples. Low laser powers (Argon 1.5%; HeNe1 6.0%) were used to minimize photobleaching and possible phototoxic effects.

Flow cytometry

Cells were cultured to 70-90% confluency, harvested, and soy bean trypsin inhibitor (Sigma-Aldrich) was added. The cells were counted by the method of Bürker and divided into test tubes (600 000 – 700 000 cells per test tube). The cells were blocked 20 min using FCS in PBS (1%), spinned down and incubated 20 – 40 minutes with biotinylated MCA-2025 (15 μg ml^{-1}) or biotinylated negative control antibody NS-1 (ATCC, a kind gift from Professors Sirpa Jalkanen and Marko Salmi, University of Turku) and washed twice with block solution. The streptavidin-coupled particles in HEPES buffer (0.1 mg ml^{-1}) were added to the tubes and incubated 30 minutes at 37 ^{o}C, then washed twice with block solution. The cells were then fixed 10 minutes in PFA/PBS (1% w/V). For trypan blue quenched samples, the cells were additionally incubated 1:1 with a trypan blue solution for 5 minutes. The flow cytometry analysis was performed in block solution (300 μl per sample) using a FACSCalibur flow cytometer (Becton Dickinson, USA).

Atomic force microscopy

Cells were prepared on 24 mm cover glasses as described above, and fixed with PFA after 15 min or 60 min incubation with the antibodies. After fixation the cells were kept in PBS. Imaging was conducted with a NanoWizard II atomic force microscope (JPK Instruments, Germany), coupled to an AxioObserver.Z1 light microscope (Carl Zeiss, Germany). The samples were kept in the BioCell sample holder (JPK Instruments, Germany) during imaging, submerged in PBS. CSC38 cantilevers (MikroMasch, Innovative Solutions Bulgaria Ltd., Bulgaria) were used in contact mode, with a low setpoint value (approximately 0.4) to minimize damage to the cells, and a scanning speed of approximately 0.3 Hz per line. A minimum of 2 randomly selected areas of 2 x 2 μm from at least 3 randomly selected cells were imaged for each sample. Unprocessed height images were saved directly from the JPK acquisition software. Additionally, 3D images of surface topography were created with the Warp Scalar 3D module of the BioImageXD software.[26]

Quantitative image analysis with BioImageXD

Colocalization was analyzed by first applying automatic background subtraction (most common value) to the non-particle channel. Then the particle channel was segmented by thresholding (manually determined value 9) and the segmented objects labeled with connected component labeling. Objects smaller than 3 voxels were filtered out as noise. Then the segmented objects were analyzed so that the average intensity of the non-particle channel was calculated within the segmented particle objects and outside them, and the ratio of these two values was calculated as the final result. To exclude background, only non-zero voxels were considered in the intensity calculations. Clustering analysis was conducted by segmenting the particle channel with the following protocol: hybrid median 2D filtering, thresholding (manually determined value 4), connected component labeling. Again, objects smaller than 3 voxels were excluded. In the analysis of the segmented objects, the following result parameters were recorded: ObjAvgIntensity, ObjAvgVolInUm, NumberOfObjects. As the number of objects is highly dependent on cell size, the cell surface area was calculated by first segmenting the cell membrane from the CellTracker channel with the following protocol: hybrid median 2D, Gaussian smoothing (4, 4, 1), thresholding (2). The result was then converted to polygonal data, and the polydata analyzed for ObjAvgAreaInUm. The number of objects obtained in the previous step was then divided by this result, to compensate for variations in cell size. Internalization was analyzed by segmenting the nanoparticles and the cell membrane as described above, and then using both segmentation results as inputs for polydata analysis (polydata image: the CellTracker result; segmented objects: the particle result). The parameters NumVoxelsInside and PercentageVoxelsInside were then calculated, to quantify how many voxels of the segmented nanoparticle objects in total were inside the segmented cell membrane at different timepoints, and how large a percentage of all nanoparticle voxels the internalized voxels represented. Delta values between timepoints 15 min and 1 h were observed. All analyses were carried out with the Procedure list task and the Batch Processor of the BioImageXD software[26], and all quantified experiments contained approximately 20 images per sample.

Preparation of figures

With the exception of the live cell imaging experiments (the purpose of which was solely visual), all results presented are based on the quantitative analyses described above, not on visual inspection of images. Nonetheless, some representative images were chosen for the display items of this article. For confocal microscopy images, linear intensity transfer function adjustments were used when needed, to improve the visibility of the image data. For merged images of two fluorescence channels, pseudocoloring was employed; otherwise confocal images are displayed in native 8-bit greyscale. All confocal images are maximum intensity projections, except Figure 5c which consists of two-channel 3D surface renderings. All images, except the table of contents entry figure, were created with the BioImageXD software.[26] The table of contents entry figure was created as a vector graphic image with Inkscape 0.48 for Windows.

Statistical analysis

Two-tailed t-tests for unequal sample sizes and unequal variances were used, after datasets had been confirmed to roughly follow normal distribution. An alpha level of 0.05 was used, and the markings with stars in the figures correspond to the following p-values: < 0.05 (*), < 0.01 (**), and < 0.001 (***).The marking "ns" means "not significant". The figure legends explain what these symbols indicate in each case. All statistical analyses were comparisons of two means, except in Figure 7, where three means were compared in each experiment, and ANOVA was therefore used in addition to the t-tests to exclude the possbility of a Type 1 error. Error bars in the figures are standard errors, except in 2a and b, and in 5c, where they show the values of the two averaged experiments.

Conclusions

We have manufactured silica-based nanoparticles that carry antibodies against α2 integrin as address labels. The advantages of using silica nanoparticles for cell-specific labeling are their biocompatibility, their synthesis that enables incorporation of tracking molecules inside the silica structure, and their relatively straightforward surface functionalization that allows fine-tuning of the particle-bioenvironment interactions. [42-44] In principle, the cellular trafficking of fluorescent nanoparticles can be followed by confocal microscopy. However, it can be challenging to combine the biological targeting activity, cargo delivery capability and imaging functionality into a single system.[35] Also, quantitative analyses of the image data are often hindered by limitations in available software,[45] especially in cases such as this, where analyses need to be highly sensitive to detect phenomena related to small and sporadic fluorescent spots. Here we have described a system where nanoparticles with specific targeting and payload delivery potential have been imaged and analyzed in detail during their entry process. Our approach is based on standard imaging methods, combined with our recently published new software, BioImageXD,[26] which we have now shown to be well suited also for nanoparticle analysis. The assays presented are sensitive enough to get around the low and varying intensities and numbers of small particles, the weak signal differences caused by multiple entry pathways, and the low resolution of light microscopy. The assays are also robust enough to be applied to similar studies of nearly any type of particles, whether natural (viruses, receptor molecules) or artificial (synthetic nanoparticles). Furthermore, due to the batch processing capabilities of BioImageXD, the assays can be run quickly and semi-automatically for very large amounts of data. All in all, BioImageXD enables optimized analyses of the various stages of the trafficking of fluorescent nanoparticles.

According to the analyses conducted, nanoparticles binding to α2β1 integrin are guided to the macropinocytotic pathway and they later accumulate into caveolin-1 positive structures. Thus, the nanoparticles seem to behave in a manner similar to human echovirus 1, a virus that uses α2β1 integrin in its entry. In general, our results suggest, together with existing literature, that different integrins could target nanoparticles to different entry pathways. This property may have a significant effect on the intracellular processing of nanoparticles and their potential cargo. Events following receptor binding should be taken into account when the properties of nanoparticles are designed.[1] For example, the pH of different intracellular vesicles and compartments varies significantly, and different pH-conditions might have some effects on particle degradation and stability. Accumulation of nanoparticles to specific locations can also provide notable advantages for targeted drug delivery.[1]

Acknowledgements

This work was supported by the Biotarget project (Contract 118196) of the Academy of Finland, the National Doctoral Programme in Informational and Structural Biology (ISB), the National Doctoral Programme in Nanoscience (NGS-NANO), Medicinska understödsföreningen liv och hälsa r.f. and K. Albin Johanssons stiftelse. L. Paavolainen and J. Päivärinne are acknowledged for assistance with the BioImageXD software, M. Tuominen for technical laboratory assistance, J. Alanko for laboratory assistance, and K. Aalto for assistance with setting up flow cytometry experiments. Flow cytometry, AFM and confocal microscopy were performed at the Cell Imaging Core, Turku Centre for Biotechnology, University of Turku and Åbo Akademi University, Turku, Finland. The research groups of the whole Biotarget project are acknowledged for creative multi-disciplinary scientific discussions.

References

1 L. Rajendran, H. Knoelker and K. Simons, Nature Reviews Drug Discovery, 2010, 9, 29-42.
2 T. WICKHAM, P. MATHIAS, D. CHERESH and G. NEMEROV, Cell, 1993, 73, 309-319).
3 M. Roivainen, T. Hyypia, L. Piirainen, N. Kalkkinen, C. Stanway and T. Hovi, J. Virol., 1991, 65, 4735-4740.
4 M. Roivainen, L. Piirainen, T. Hovi, I. Virtanen, T. Riikonen, J. Heino and T. Hyypia, Virology, 1994, 203, 357-365.
5 C. Williams, T. Kajander, T. Hyypia, T. Jackson, D. Sheppard and G. Stanway, J. Virol., 2004, 78, 6967-6973.
6 P. Joki-Korpela, V. Marjomaki, C. Krogerus, J. Heino and T. Hyypia, J. Virol., 2001, 75, 1958-1967.
7 G. Fox, N. Parry, P. Barnett, B. Mcginn, D. Rowlands and F. Brown, J. Gen. Virol., 1989, 70, 625-637).
8 S. Akula, N. Pramod, F. Wang and B. Chandran, Cell, 2002, 108, 407-419.
9 M. V. Veettil, S. Sadagopan, N. Sharma-Walia, F. Wang, H. Raghu, L. Varga and B. Chandran, J. Virol., 2008, 82, 12126-12144.
10 J. Bergelson, M. Shepley, B. Chan, M. Hemler and R. Finberg, Science, 1992, 255, 1718-1720.
11 J. Jokinen, D. J. White, M. Salmela, M. Huhtala, J. Kapyla, K. Sipila, J. S. Puranen, L. Nissinen, P. Kankaanpaa, V. Marjomaki, T. Hyypia, M. S. Johnson and J. Heino, EMBO J., 2010, 29, 196-208.
12 V. Marjomaki, V. Pietiainen, H. Matilainen, P. Upla, J. Ivaska, L. Nissinen, H. Reunanen, P. Huttunen, T. Hyypia and J. Heino, J. Virol., 2002, 76, 1856-1865.
13 P. Upla, V. Marjomaki, P. Kankaanpaa, J. Ivaska, T. Hyypia, F. van der Goot and J. Heino, Mol. Biol. Cell, 2004, 15, 625-63

14 M. Karjalainen, E. Kakkonen, P. Upla, H. Paloranta, P. Kankaanpaa, P. Liberali, G. H. Renkema, T. Hyypia, J. Heino and V. Marjomaki, Mol. Biol. Cell, 2008, 19, 2857-2869.
15 P. D. Arora, M. A. Conti, S. Ravid, D. B. Sacks, A. Kapus, R. S. Adelstein, A. R. Bresnick and C. A. McCulloch, Mol. Biol. Cell, 2008, 19, 5032-5046.
16 J. Hood, M. Bednarski, R. Frausto, S. Guccione, R. Reisfeld, R. Xiang and D. Cheresh, Science, 2002, 296, 2404-2407.
17 E. A. Murphy, B. K. Majeti, L. A. Barnes, M. Makale, S. M. Weis, K. Lutu-Fuga, W. Wrasidlo and D. A. Cheresh, Proc. Natl. Acad. Sci. U. S. A., 2008, 105, 9343-9348.
18 H. S. Choi, W. Liu, F. Liu, K. Nasr, P. Misra, M. G. Bawendi and J. V. Frangioni, Nature Nanotechnology, 2010, 5, 42-47.
19 M. Benezra, O. Penate-Medina, P. B. Zanzonico, D. Schaer, H. Ow, A. Burns, E. DeStanchina, V. Longo, E. Herz, S. Iyer, J. Wolchok, S. M. Larson, U. Wiesner and M. S. Bradbury, J. Clin. Invest., 2011, 121, 2768-2780.
20 M. Shokeen, E. D. Pressly, A. Hagooly, A. Zheleznyak, N. Ramos, A. L. Fiamengo, M. J. Welch, C. J. Hawker and C. J. Anderson, Acs Nano, 2011, 5, 738-747.
21 A. H. Schmieder, S. D. Caruthers, H. Zhang, T. A. Williams, J. D. Robertson, S. A. Wickline and G. M. Lanza, Faseb Journal, 2008, 22, 4179-4189.
22 K. Shroff and E. Kokkoli, Langmuir, 2012, 28, 4729-4736.
23 W. Dai, T. Yang, Y. Wang, X. Wang, J. Wang, X. Zhang and Q. Zhang, Nanomedicine-Nanotechnology Biology and Medicine, 2012, 8, 1152-1161.
24 K. Xiao, Y. Li, J. S. Lee, A. M. Gonik, T. Dong, G. Fung, E. Sanchez, L. Xing, H. R. Cheng, J. Luo and K. S. Lam, Cancer Res., 2012, 72, 2100-2110.
25 W. Stober, A. Fink and E. Bohn, J. Colloid Interface Sci., 1968, 26, 62-.
26 P. Kankaanpaa, L. Paavolainen, S. Tiitta, M. Karjalainen, J. Paivarinne, J. Nieminen, V. Marjomaki, J. Heino and D. J. White, Nature Methods, 2012, 9, 683-689.
27 J. Ivaska, H. Reunanen, J. Westermarck, L. Koivisto, V. Kahari and J. Heino, J. Cell Biol., 1999, 147, 401-415.
28 M. Zutter and S. Santoro, Am. J. Pathol., 1990, 137, 113-120.
29 M. Boisvert, N. Chetoui, S. Gendron and F. Aoudjit, Eur. J. Immunol., 2010, 40, 2710-2719.
30 D. Senger, K. Claffey, J. Benes, C. Perruzzi, A. Sergiou and M. Detmar, Proc. Natl. Acad. Sci. U. S. A., 1997, 94, 13612-13617.
31 A. Collins, F. Habib, N. Maitland and D. Neal, J. Cell. Sci., 2001, 114, 3865-3872.
32 N. Gagliani, C. F. Magnani, S. Huber, M. E. Gianolini, M. Pala, P. Licona-Limon, B. Guo, D. R. Herbert, A. Bulfone, F. Trentini, C. Di Serio, R. Bacchetta, M. Andreani, L. Brockmann, S. Gregori, R. A. Flavell and M. Roncarolo, Nat. Med., 2013, 19, 739-.
33 K. Chuang, H. Wang, F. Chen, S. Tzou, C. Cheng, Y. Chang, W. Tseng, J. Shiea, S. Lin, J. Wang, B. Chen, S. R. Roffler and T. Cheng, Molecular Cancer Therapeutics, 2010, 9, 1903-1912.
34 I. Slowing, B. G. Trewyn and V. S. -. Lin, J. Am. Chem. Soc., 2006, 128, 14792-14793.
35 J. M. Rosenholm, A. Meinander, E. Peuhu, R. Niemi, J. E. Eriksson, C. Sahlgren and M. Linden, Acs Nano, 2009, 3, 197-206.
36 T. Luehmann, M. Rimann, A. G. Bitterman and H. Hall, Bioconjug. Chem., 2008, 19, 1907-1916.
37 A. I. Ivanov, Methods Mol. Biol., 2008, 440, v-vi.
38 J. Heino and J. Kapyla, Curr. Pharm. Des., 2009, 15, 1309-1317.
39 B. Yameen, W. I. Choi, C. Vilos, A. Swami, J. Shi and O. C. Farokhzad, J. Controlled Release, 2014, 190, 485-499.
40 M. Salmi and S. Jalkanen, Science, 1992, 257, 1407-1409 .
41 P. Nykvist, H. M. Tu, J. Ivaska, J. Kapyla, T. Pihlajaniemi and J. H. Heino, J. Biol. Chem., 2000, 275, 8255-8261 .
42 F. Hoffmann, M. Cornelius, J. Morell and M. Froeba, Angewandte Chemie-International Edition, 2006, 45, 3216-3251.
43 J. Kecht, A. Schlossbauer and T. Bein, Chemistry of Materials, 2008, 20, 7207-7214.
44 L. Bergman, J. Rosenholm, A. Ost, A. Duchanoy, P Kankaanpaa, J. Heino and M. Linden, Journal of Nanomaterials, 2008, , 712514.
45 T. Walter, D. W. Shattuck, R. Baldock, M. E. Bastin, A. F Carpenter, S. Duce, J. Ellenberg, A. Fraser, N. Hamilton, S Pieper, M. A. Ragan, J. E. Schneider, P. Tomancak and Heriche, Nature Methods, 2010, 7, S26-S41.